Journal of Power Sources 222 (2013) 230–236

Contents lists available at SciVerse ScienceDirect

Journal of Power Sources

journal homepage: www.elsevier.com/locate/jpowsour

Ionic conductivity investigation in lanthanum (La) and strontium (Sr) co-doped ceria system

Nandini Jaiswal [a], Shail Upadhyay [b], Devendra Kumar [a], Om Parkash [a,*]

[a] Department of Ceramic Engineering, Indian Institute of Technology (Banaras Hindu University), Varanasi 221005, India
[b] Department of Applied Physics, Indian Institute of Technology (Banaras Hindu University), Varanasi 221005, India

HIGHLIGHTS

- The system $Ce_{1-x-y}La_xSr_yO_{2-\{x/2+y\}}$ has been investigated for the first time.
- In present study, number of oxygen vacancies is kept constant in all composition.
- Composition $Ce_{0.89}La_{0.07}Sr_{0.04}O_{1.925}$ has maximum conductivity more than highest conductivity reported in SDC and GDC at 600 °C.
- It is much less costly than that of SDC and GDC.
- This makes CL7S4 is a potential candidate as a solid electrolyte for ITSOFCs.

ARTICLE INFO

Article history:
Received 18 June 2012
Received in revised form
29 August 2012
Accepted 31 August 2012
Available online 10 September 2012

Keywords:
Doped ceria
Combustion synthesis
Co-doping effect
Impedance analysis
Electrical conductivity

ABSTRACT

Effect of strontium doping on ionic conductivity of lanthanum-doped ceria has been investigated. Distribution and average radius of oxygen vacancies formed from divalent and trivalent dopant cations in co-doped system has been calculated using hard-sphere model. Phase identification, microstructure and ionic conductivities of samples have been studied by X-ray diffraction (XRD), scanning electron microscopy (SEM), and AC impedance spectroscopy, respectively. X-ray diffraction reveals that all the samples are single phase with cubic fluorite-type structure. Dense ceramics with density ~95% of the theoretical density have been obtained without using any sintering aid. The results show that the samples co-doped with La and Sr exhibit higher ionic conductivity and lower activation energy than those of ceria doped with La only in the intermediate temperature range. The highest ionic conductivity has been observed for $Ce_{0.89}La_{0.07}Sr_{0.04}O_{1.925}$ in the samples investigated (4.01×10^{-3} S cm^{-1}) at 500 °C, which is 20 times as high as that of $Ce_{0.85}La_{0.15}O_{1.925}$. Concept of average oxygen vacancy radius has been found to be a useful in calculating the lattice parameter in this system.

1. Introduction

Solid oxide fuel cells (SOFCs) are considered as an alternative electric power generation systems due to high energy conversion efficiency, fuel flexibility and operation directly on natural gas [1–5]. Application of SOFCs is, however, still limited because of high cost of component materials. The SOFC-based generators can be commercially viable only if their production cost drops [2,3]. This can be done through development of new materials as solid electrolytes because these are the key components of electrochemical cells [5]. Solid electrolytes should have numerous requirements, such as high oxide ion conductivity, negligible electronic conduction and thermodynamically stability over a wide range of temperature and oxygen partial pressure. Doped ceria is a well known material in modern ceramics because of its high oxide ionic conductivity for the fabrication of fuel cells and oxygen sensors [6].

An increase of oxygen vacancies in ceria enhances the ionic conductivity. The vacancies are not, however, free; these are associated with dopant cations leading to decrease in ionic conductivity beyond a particular concentration. For example, 20 mol% of rare earth dopants produce sufficient concentration of oxygen vacancies in samarium doped ceria, $Ce_{0.80}Sm_{0.20}O_{1.90}$ (SDC) [2] and gadolinium doped ceria $Ce_{0.80}Gd_{0.20}O_{1.90}$ (GDC) systems [3]. If the content of the trivalent dopant exceeds 20 mol %, then the ionic conductivity decreases due to defect association and/or clustering of oxygen vacancies. Ionic radius of the dopant also affects the ionic conductivity. If the difference in the ionic

* Corresponding author. Tel.: +91 542 6701791; fax: +91 542 2368428.
E-mail address: oprakash.cer@itbhu.ac.in (O. Parkash).

0378-7753/$ – see front matter © 2012 Elsevier B.V. All rights reserved.
http://dx.doi.org/10.1016/j.jpowsour.2012.08.095

radius of the dopant and host ion (Ce^{4+}) is large, then large strain is induced in the lattice and the ionic conductivity decreases. Compatibility of ionic radius of the dopant and the host cation is very critical in achieving the desired lattice match and, thereby, the properties. Moreover, the lattice binding energy of dopant should be low. Thus, taking into consideration these critical factors, enhancement of the ionic conductivity has been achieved by suitable dopants.

Co-doping has been reported as a novel method to increase the ionic conductivity of ceria [4,5,7–15]. The results reported on co-doped and singly doped ceria are however, controversial in nature. For example, Herle et al. [16] found that co-doped ceria with 3,5 or 10 dopants show higher ionic conductivity than the best singly doped materials whereas Yoshida et al. [17,18] did not find additive effect of La^{3+} and Y^{3+} co-doping on the ionic conductivity of ceria. $Ce_{0.80}Gd_{0.2-x}Pr_xO_{1.9}$ [19], $Ce_{0.80}Gd_{0.2-x}Sm_xO_{1.9}$ [20] and $Ce_{0.85}Gd_{0.1}Mg_{0.05}O_{1.9}$ [21] electrolytes provide evidence for enhancement of the ionic conductivity due to co-doing. It is found that ionic conductivity of a co-doped system is sometimes more while other times less than that of a singly doped ceria. Systematic research has been done on samarium and strontium co-doped ceria by Yeh and Chou [22] who found that $Ce_{0.78}Sm_{0.20}Sr_{0.02}O_{1.88}$ has the highest ionic conductivity (6.1×10^{-2} S-cm^{-1}) at 800 °C. These authors ascribed the enhancement in the conductivity to the increase in number of oxygen vacancies, decrease in the association enthalpy and increase in radii of oxygen vacancies which widen the channels for easy movement of oxygen ions.

In the present investigations, effect of double substitution of La^{3+} and Sr^{2+} on the electrical properties of ceria has been studied. Nanocrystalline $Ce_{0.85}La_{0.15}O_{1.925}$ (CLO15), $Ce_{0.87}La_{0.11}Sr_{0.02}O_{1.925}$ (CL11S2), $Ce_{0.89}La_{0.07}Sr_{0.04}O_{1.925}$ (CL7S4), and $Ce_{0.91}La_{0.03}Sr_{0.06}O_{1.925}$ (CL3S6) having same number of total oxygen vacancies have been prepared using citrate-nitrate auto-combustion method. A significant improvement of the electrical conductivity is observed by co-doping ceria with lanthanum and strontium.

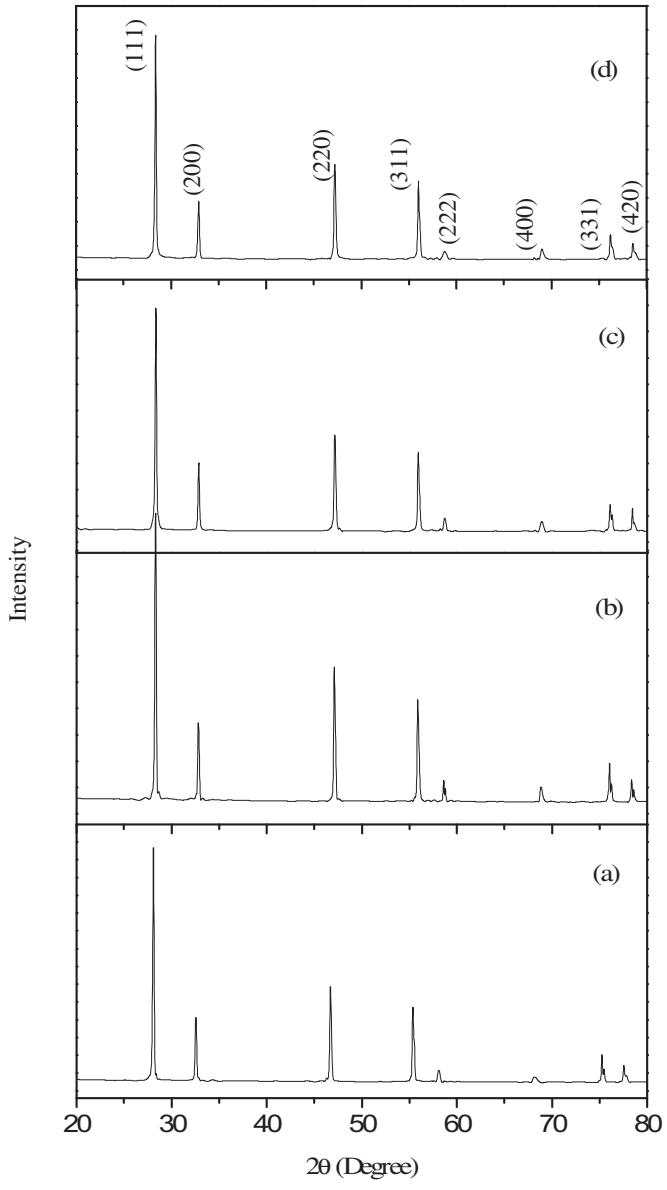

Fig. 1. Powder X-ray diffraction patterns of various compositions (a) CLO15, (b) CL11S2, (c) CL7S4, (d) CL3S6 sintered at 1350 °C.

2. Experimental

A series of samples having general formula $Ce_{1-x-y}La_xSr_yO_{2-\{x/2+y\}}$ where $\{(x = 0.15, y = 0), (x = 0.11, y = 0.02), (x = 0.07, y = 0.04)$ and $(x = 0.03, y = 0.06)\}$ were synthesized by citrate–nitrate auto-combustion method. Starting chemicals used for the synthesis of powders were ammonium ceric nitrate (purity 99%), lanthanum oxide, strontium nitrate, and citric acid. Reaction solution consisted of Ce-nitrate, La-nitrate, Sr-nitrate (purity 99.5%), and citric acid (purity>99%), in the ratio depending on the final composition. Citrate to nitrate molar ratio in the solution was kept constant as 0.3 [23]. The solution was concentrated on a hot plate at 200 °C until excess free water evaporated and the final spontaneous ignition occurred. Within a few seconds, the combustion reaction completed with yellow porous ash filling the container. During the ignition, the container was covered with a fine-mesh sieve to prevent the ash from flying out of the container. The as-collected ash was calcined at 800 °C in air for 4 h. The calcined powders were uniaxially dry-pressed into pellets (about 15 mm in diameter and 1.5 mm thick) without any binder by applying 50 kN load into a cylindrical shape. The pellets were sintered at 1350 °C for 4 h.

Crystal structure was determined using a Rigaku high resolution powder X-ray diffractometer employing Cu $K_{\alpha 1}$ radiation and Ni-filter at room temperature. Data were collected in the Bragg angle range of $20° \leq 2\theta \leq 80°$. The crystallite size, D was estimated using Scherrer's formula

$$D = \frac{0.9\lambda}{\beta \cos\theta} \quad (1)$$

where β is the full width at half maxima (FWHM) excluding instrumental broadening, λ is the wave length of X-ray diffraction and θ is the Bragg angle. β is taken for the strongest Bragg's peak corresponding to (111) reflection for all the samples. Lattice parameters were calculated using 'Cell' software. Density of sintered pellets was determined by Archimedes method and expressed as percentage of the theoretical values determined from the cubic lattice parameter and molecular weight of sample. Sintered pellets were polished using emery papers of grade 1/0, 2/0, 3/0, and 4/0 (Sia, Switzerland) followed by polishing on a velvet cloth with diamond paste of grade1/4-OS-475 (HIFIN). Then these were etched thermally at 1250 °C. Micrographs were taken with the help of a scanning electron microscope (INSPECT 50 FEI').

Electrical conductivity of the materials was measured using sintered pellets. Silver paste was used as electrodes on both the surfaces of each pellet. Impedance was measured using a Novocontrol Alpha-A High Performance Frequency Analyzer with an

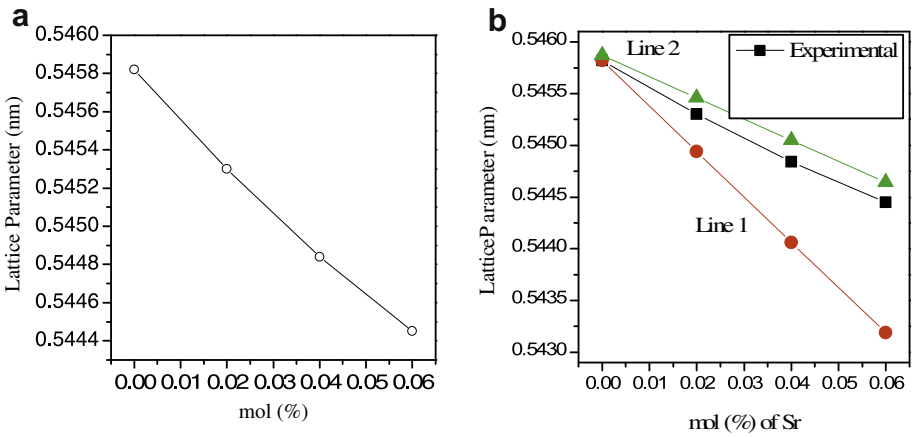

Fig. 2. (a) Variation of lattice parameter as a function of the dopant concentration for the system $Ce_{1-x-y}La_xSr_yO_{2-\{x/2+y\}}$. (b) Calculated results and experimental data for the lattice parameter of lanthanum and strontium co-doped ceria systems as a function of Sr content.

applied voltage of 20 mV. The measurements were made in air in the temperature range 200–500 °C at different frequencies in the range 1 Hz to 1 MHz.

3. Results and discussion

Powder X-ray diffraction of as-prepared ash shows the formation of a single phase solid solution having fluorite structure similar to CeO_2, suggesting that Ce ions are in the 4+ state in the as-prepared ash. If the Ce ions were present in the +3 state in the precursor, one would expect the formation of Ce_2O_3 instead of CeO_2. XRD patterns for the calcined powders are similar to those obtained after sintering except that the diffraction lines become sharper as shown in Fig. 1. This is due to grain growth occurring during sintering. Fig. 1 also shows that the 2θ values of co-doped ceria shifts slightly towards lower angles with Sr content. Diffraction patterns were indexed on the basis of fluorite structure similar to CeO_2 using JCPDS file no. 43-1002. The lattice constant was determined using "Cell" software.

Lattice constant increases from 5.4019 ± 0.0016 Å [24] to 5.4582 ± 0.0005 Å on addition of La to CeO_2. This can be attributed to the volume expansion of lattice due to larger ionic radius of La^{3+} (1.16 Å) in comparison to Ce^{4+} (0.97 Å). The bond length of the ceria matrix (Ce–O/Ce-cations) increases on addition of lanthanum since its lattice binding energy with oxygen ion is lower than the ceria matrix [22]. Doping of La^{3+} in ceria lattice will also induce a strain in the lattice as the material is elastically deformed. Lattice constant decreased linearly with increasing concentration of Sr^{2+}as shown in Fig. 2(a). This is due to decrease in the total concentration of dopants, i.e. for each mol% of Sr^{2+}, 2 mol% of La^{3+} decreases. Average crystallite size, D, of powders, calculated by Scherrer's formula from the X-ray line broadening is between 53 and 69 nm (Table 1). Pellets sintered at 1350 °C have density more than 95% of the theoretical values (Table 1).

Table 1
Crystallite size, lattice parameter and % theoretical density of compositions of the system $Ce_{1-x-y}La_xSr_yO_{2-\{x/2+y\}}$.

S.No.	Compositions	Crystallite size of sintered powder (nm)	Lattice parameter (Å)	% of theoretical density
1.	$Ce_{0.85}La_{0.15}O_{1.925}$	53	5.4582 ± 0.0005	98.3
2.	$Ce_{0.87}La_{0.11}Sr_{0.02}O_{1.925}$	58	5.4530 ± 0.0003	97.7
3.	$Ce_{0.89}La_{0.07}Sr_{0.04}O_{1.925}$	57	5.4484 ± 0.0005	95.0
4.	$Ce_{0.91}La_{0.03}Sr_{0.06}O_{1.925}$	69	5.4445 ± 0.0011	94.3

The lattice parameters of lanthanum and strontium co-doped ceria system ($Ce_{1-x-y}La_xSr_yO_{2-\{x/2+y\}}$) were calculated by hard sphere model [25]. The equation of $Ce_{1-x-y}La_xSr_yO_{2-\{x/2+y\}}$ system can be written as:

$$xLaO_{1.5} + ySrO + (1-x-y)CeO_2 = xLa'_{Ce} + ySr''_{Ce} + \left(\frac{x}{2}+y\right)V_{\ddot{O}} + (1-x-y)Ce_{Ce} + [2-(x/2+y)]O_o \quad (2)$$

where the species are written in accordance with Kroger Vink notation of defects. Lattice parameter of an ideal fluorite structure can be calculated using Eq. (3):

$$a = \frac{4}{\sqrt{3}}(r_{anion} + r_{cation}) \quad (3)$$

where r_{anion} and r_{cation} are radii of the dopant cations and anions, respectively. The radii of cation and anion can be calculated using the following Eqs. (4) and (5):

$$r_{cation} = xr_{La} + yr_{Sr} + (1-x-y)r_{Ce} \quad (4)$$

$$r_{anion} = \left(\frac{2-\left(\frac{x}{2}+y\right)}{2}\right)r_o + \left(\frac{\frac{x}{2}+y}{2}\right)r_{V_{\ddot{o}}} \quad (5)$$

where r_{Ce}, r_{Sr}, r_{La}, $r_{V_{\ddot{o}}}$ and r_o are radii of Ce^{4+}, dopant cations, oxygen vacancy and oxygen ion, respectively.

From the above equations, lattice parameter of lanthanum and strontium co-doped ceria system can be written as:

$$a = \frac{4}{\sqrt{3}}(r_{anion} + r_{cation}) = \frac{4}{\sqrt{3}}\left[xr_{La} + yr_{Sr} + (1-x-y)r_{Ce} + \left(\frac{2-\left\{\frac{x}{2}+y\right\}}{2}\right)r_o + \left(\frac{x}{4}r_{V_{\ddot{O}_t}} + 0.5yr_{V_{\ddot{O}_d}}\right)\right] \quad (6)$$

By using $r_{Ce} = 0.97$ Å, and $r_o = 1.4$ Å, lattice parameter of CeO_2 is found to be 5.473 Å. Since the actual lattice parameter of pure ceria is 5.414 Å from JCPDS files, a multiplication factor of 5.414/

5.473 = 0.9892 was taken in all of the above equations [26]. Hence, the equation for lattice parameter can be written as:

$$a = 0.9892 \times \frac{4}{\sqrt{3}}\left[xr_{La} + yr_{Sr} + (1-x-y)r_{Ce} + \left(\frac{2-\left\{\frac{x}{2}+y\right\}}{2}\right)r_o + \left(\frac{x}{4}r_{V_{\ddot{O}_t}} + 0.5yr_{V_{\ddot{O}_d}}\right)\right] \quad (7)$$

where $V_{\ddot{O}_t}$ and $V_{\ddot{O}_d}$ are oxygen vacancy produced from trivalent and divalent cations, respectively. Eq. (7) was used to determine theoretical value of lattice parameter for lanthanum and strontium co-doped ceria solid solutions. Lattice parameter for $Ce_{0.90}Sr_{0.10}O_{1.90}$ and $Ce_{0.85}La_{0.15}O_{1.925}$ can be calculated using Eqs. (8) and (9).

(a) $Ce_{0.90}Sr_{0.10}O_{1.90}$

$$a = 0.9892 \times \frac{4}{\sqrt{3}}\left[0.90r_{Ce} + 0.10r_{Sr} + \left(\frac{1.9}{2}\right)r_o + \left(\frac{0.10}{2}\right)r_{V_{\ddot{O}}}\right] \quad (8)$$

(b) $Ce_{0.85}La_{0.15}O_{1.925}$

$$a = 0.9892 \times \frac{4}{\sqrt{3}}\left[0.85r_{Ce} + 0.15r_{La} + \left(\frac{1.925}{2}\right)r_o + \left(\frac{0.075}{2}\right)r_{V_{\ddot{O}}}\right] \quad (9)$$

Substituting the lattice parameter of $Ce_{0.90}Sr_{0.10}O_{1.90}$ (5.429 Å) and $Ce_{0.85}La_{0.15}O_{1.925}$ (5.4582 Å) in Eqs. (8) and (9), calculated oxygen vacancy radii of $Ce_{0.90}Sr_{0.10}O_{1.90}$ and $Ce_{0.85}La_{0.15}O_{1.925}$ are 0.9498 and 1.154 Å, respectively.

The calculated results and experimental data of lattice parameters of lanthanum and strontium co-doped ceria systems are plotted as shown in Fig. 2(b).

Substituting the values of ionic radius of oxygen vacancy produced by trivalent and divalent dopant denoted by $r_{V_{\ddot{O}_t}}$ and $r_{V_{\ddot{O}_d}}$ as 1.154 and 0.9498 Å, respectively, in Eq. (7), the lattice parameters were calculated and are shown by line 1 in Fig. 2(b). These calculated values are different from the lattice parameter obtained from the experimental data as shown in Fig. 2(b). If the same value of $r_{V_{\ddot{O}_t}}$ and $r_{V_{\ddot{O}_d}}$ (average oxygen vacancy radius 1.16 Å) are substituted in Eq. (7), the calculated results of lattice parameter are shown by line 2. This result was found in good agreement with the experimental result. Therefore, it is found that the radii of oxygen vacancies formed by trivalent and divalent cations in lanthanum and strontium co-doped ceria systems are not different. These results are different from the results obtained by Yeh and Chou [22], where they found that radii of oxygen vacancies created by divalent and trivalent dopants are different.

Fig. 3(a)–(d) shows micrographs of thermally etched samples at 1250 °C. The surface micrograph of sintered pellets revealed a dense structure and well defined grains separated by grain boundaries. All the samples show grains having varying shape and size. The image of all the samples except CLO15 indicates the presence of faceted grains. It is interesting to notice that average grain size increases with increasing concentration of strontium up to 4 mol% and thereafter it decreases. The average grain size for the samples CLO15, CL11S2, CL7S4 and CL3S6 are found to be 1.0, 3.5, 4.0 and 2.9 μm, respectively.

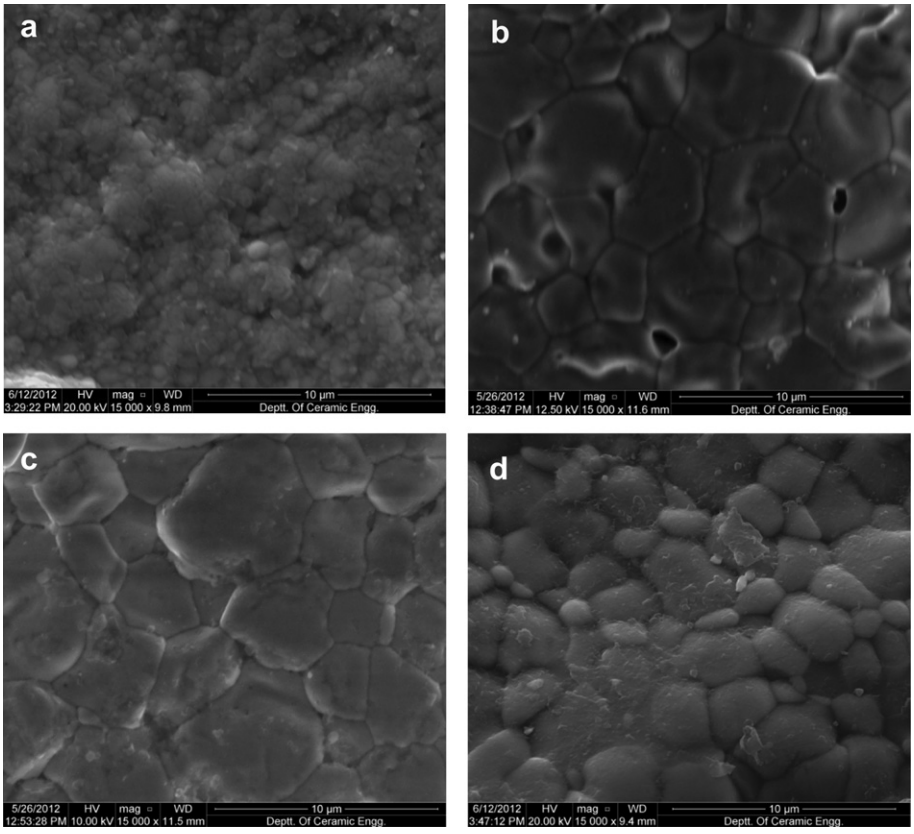

Fig. 3. Scanning electron micrographs of various compositions (a) CLO15, (b) CL11S2, (c) CL7S4, (d) CL3S6 etched at 1250 °C.

AC impedance analysis is well suited for the electrical conductivity measurements of ionic conductors. This method provides information on the contribution of grains and grain boundaries and electrode polarization to the total conductivity.

Complex plane impedance plots of all the samples in air at 200 °C as well as for CL7S4 sample at different temperatures are shown in Fig. 4a and b, respectively. At 200 °C, three contributions can be distinguished: an incomplete depressed semicircle at high frequency and two depressed arcs at lower frequencies. These arcs can be ascribed to contribution of grain polarization, grainboundary polarization, and electrodes polarization, respectively in order of decreasing frequency. In order to see clearly, the contribution of grains, the data is plotted on an expanded scale in the insets. Intercepts of the arcs due to grains and grain boundaries decrease with increase in Sr^{2+} concentration for $y \leq 0.04$. Thereafter these values decrease for $y > 0.04$. The time constant τ, for a dielectric relaxation decreases as temperature increases. This leads to shifting of arcs towards higher frequencies. Therefore, all the arcs are not observed at all temperatures in the limited range of frequency of the equipment. The arc corresponding to contribution of grains disappears at 325 °C. It is noted from Fig. 4(a) that total resistance given by $R_g + R_{gb}$ is minimum for CL7S4 among all the compositions. Arcs due to grains and grain boundaries are associated with the capacitances in the pF and nF ranges, respectively, determined from $2\pi f_{max} RC = 1$, where f_{max} is the applied frequency at the arc maximum and R is the resistance obtained from the intercept of the arcs on Z' axis. Total resistance of the electrolyte is given by:

$$R_t = R_g + R_{gb} \tag{10}$$

Conductivity σ at different temperatures can be obtained using the formula:

$$\sigma = \frac{L}{S \times R} \tag{11}$$

where L and S represent the thickness and electrode area of the sample surface, respectively.

Addition of trivalent or divalent cations to ceria produces oxygen vacancies responsible for ionic conduction in these oxides [27–29] as given below in the Eqs. (12) and (13).

$$La_2O_3 \xrightarrow{2CeO_2} 2La'_{Ce} + 3O_O + V_O^{\bullet\bullet} \tag{12}$$

$$SrO \xrightarrow{CeO_2} Sr''_{Ce} + O_O + V_O^{\bullet\bullet} \tag{13}$$

where all the species are written in accordance with Kroger Vink notation.

Arrhenius plots of bulk conductivity for all the samples are shown in Fig. 5. Ionic conductivity of grains increases with increasing strontium content up to 4 mol%. For higher concentration of Sr^{2+} ($y > 0.04$) it decreases. This is probably due to the dissolution of SrO in the ceria. Dissolution of Sr^{2+} ions in lanthanum-doped ceria sample will produce a higher association enthalpy for oxygen vacancies and hence lower conductivity [29]

Arrhenius plots of grain boundary conductance of the samples are shown in Fig. 6. It can be seen from Fig. 6 that the grain boundaries conductance of the samples depends strongly on the Sr content. It may be due to scavenging effect of Sr^{2+} ions to remove siliceous impurities. It has been reported by Gerhardt et al. [30], on the basis of scanning transmission electron microscopy (STEM) combined with energy dispersive X-ray microanalysis (EDXM) and electron energy loss spectroscopy (EELS) that in yttrium doped ceria there exists an amorphous silica thick layer surrounding the grains. This layer blocks the charge carriers leading to increase in

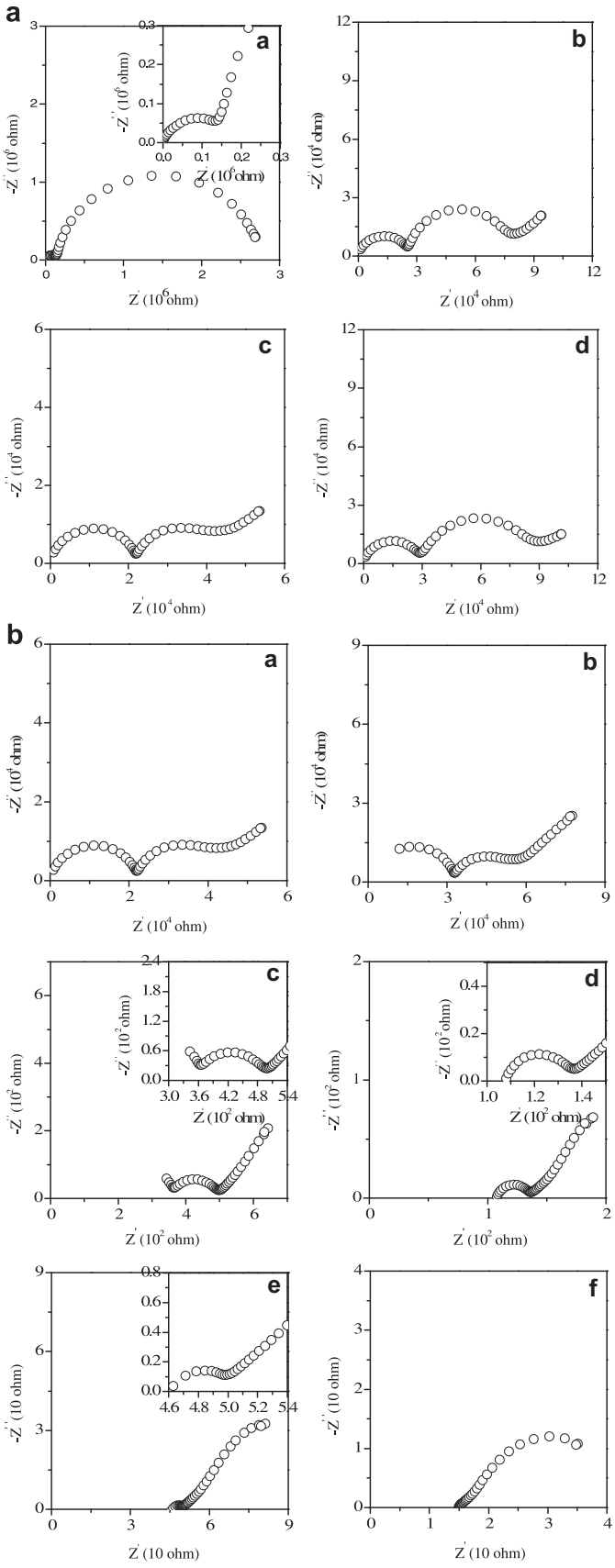

Fig. 4. (a) Impedance plots for various compositions (a) CLO15, (b) CL11S2, (c) CL7S4, (d) CL3S6 at 200 °C. (b) Impedance plots for the composition CL7S4 at (a) 200 °C, (b) 250 °C, (c) 325 °C, (d) 375 °C, (e) 425 °C and (f) 500 °C.

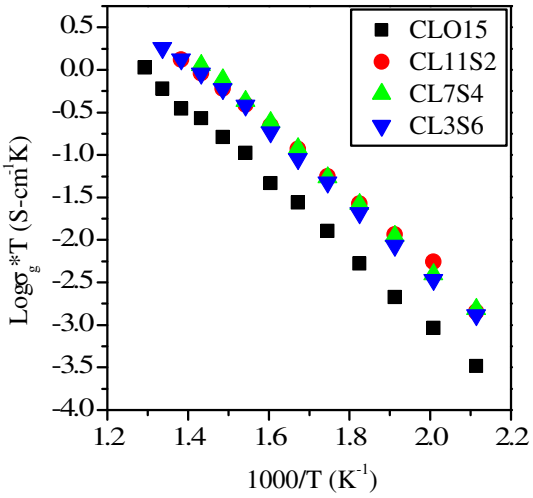

Fig. 5. log $\sigma_g \cdot T$ vs 1000/T plots of all the compositions of the system $Ce_{1-x-y}La_xSr_yO_{2-\{x/2+y\}}$.

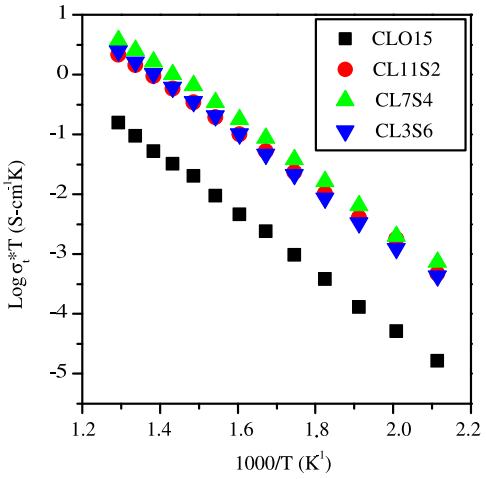

Fig. 7. log $\sigma_t \cdot T$ vs 1000/T plots of all the compositions of the system $Ce_{1-x-y}La_xSr_yO_{2-\{x/2+y\}}$.

the resistivity of the grain boundaries and hence the total resistivity. They also observed the formation of some silicate phases of yttrium. Similar silicate phases may form in the materials under present investigation. The exact compositions, morphology and distribution of these phases require analytical studies as mentioned above. Removal of silica decreases the resistivity of the grain boundaries leading to decrease in the total resistivity. They further observed that increase in ionic radius of the dopant increases its effectiveness in removing silica [31]. To confirm the scavenging effect of strontium for grain boundaries, the influence of the grain boundaries conductivity on the total conductivity is evaluated through the blocking factor (α_R) [31,32] given by

$$\alpha_R = \frac{R_{gb}}{R_g + R_{gb}} \tag{14}$$

where R_g and R_{gb} are resistance of grains and grain boundaries. α_R gives the fraction of charge carriers being blocked at the impermeable internal surface, under the measuring conditions, with respect to the total number of charge carriers in the samples. The blocking factor is minimum for the sample CL7S4 (0.21) at 375 °C.

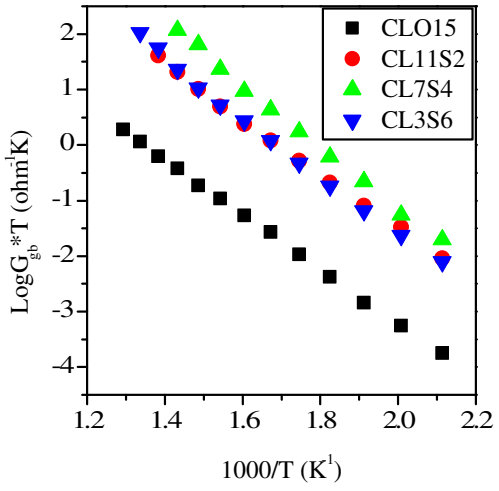

Fig. 6. log $G_{gb} \cdot T$ vs 1000/T plots of all the compositions of the system $Ce_{1-x-y}La_xSr_yO_{2-\{x/2+y\}}$.

For CLO15 its value at 375 °C is 0.90. This establishes that strontium is an effective grain boundaries scavenger.

Fig. 7 shows Arrhenius plots of the total ionic conductivity for the samples. Activation energy of conduction for the total conductivity was determined by fitting the conductivity data to the Arrhenius relation:

$$\sigma = \frac{A}{T} \exp - \frac{E}{kT} \tag{15}$$

where E is the activation energy for migration of O^{2-} ions, k is the Boltzman's constant, T is temperature in Kelvin, and A is the pre-exponential factor. Activation energies for conduction, calculated from the slopes of Arrhenius plots in the temperature range 200–500 °C are given in Table 2. It can be seen that the activation energies for conduction in co-doped ceria are less than those of ceria doped with La only.

It is found that addition of strontium improves the ionic conductivity. The composition $Ce_{0.89}La_{0.07}Sr_{0.04}O_{1.925}$ (CL7S4) shows the highest total conductivity among all the samples. Surprisingly, the ionic conductivity of $Ce_{0.89}La_{0.07}Sr_{0.04}O_{1.925}$ (CL7S4), (4.76×10^{-3} S-cm^{-1}) is about 20 times as high as that of $Ce_{0.85}La_{0.15}O_{1.925}$ (CLO15) (2.02×10^{-4} S-cm^{-1}) at 500 °C. It suggests that co-doping using an optimum ratio of La^{3+} and Sr^{2+} concentration enhances the ionic conductivity. Ionic conductivity of $Ce_{0.89}La_{0.07}Sr_{0.04}O_{1.925}$ at 600 °C (obtained by extrapolation) is more (Table 2) than the reported values of conductivity for compositions $Ce_{0.8}Sm_{0.2}O_{1.90}$ (1.20×10^{-2} S-cm^{-1}) [33] and $Ce_{0.8}Gd_{0.2}O_{1.90}$ (1.29×10^{-2} S-cm^{-1}) [34] at 600 °C.

In this study, the partial substitution of La with Sr causes four effects for the samples of $Ce_{1-x-y}La_xSr_yO_{2-\{x/2+y\}}$. Yamamura et al. [35] reported that the ordering of oxygen vacancies is suppressed

Table 2
Total conductivity (at 500 °C and 600 °C), activation energy of grains (E_g), grain-boundaries (E_{gb}) and total (E_t) conductivity of various compositions of the system $Ce_{1-x-y}La_xSr_yO_{2-\{x/2+y\}}$.

S.No.	Compositions	σ_t at 500 °C (S cm^{-1})	σ_t at 600 °C (S cm^{-1})[a]	E_g (eV)	E_{gb} (eV)	E_t (eV)
1.	$Ce_{0.85}La_{0.15}O_{1.925}$	2.02×10^{-4}	9.400×10^{-4}	0.89	0.98	0.97
2.	$Ce_{0.87}La_{0.11}Sr_{0.02}O_{1.925}$	2.79×10^{-3}	1.230×10^{-2}	0.79	0.98	0.88
3.	$Ce_{0.89}La_{0.07}Sr_{0.04}O_{1.925}$	4.75×10^{-3}	2.370×10^{-2}	0.85	1.11	0.91
4.	$Ce_{0.91}La_{0.03}Sr_{0.06}O_{1.925}$	3.19×10^{-3}	1.497×10^{-2}	0.83	1.05	0.92

[a] Data obtained by extrapolation.

due to doping. This decreases activation energy which enhances the conductivity. The number of $[La'_{Ce} - V_O^{\cdot\cdot}]^{\cdot}$ pairs decreases as twice the number of Sr^{2+} ions added. This decreases total number of associated pairs leading to enhancement of the ionic conductivity. Replacement of La^{3+} by Sr^{2+} increases the lattice strain [36] due to larger size of Sr^{2+} ion (1.26 Å) as compared to La^{3+} ion (1.16 Å). This causes the increase in association enthalpy of dopant–vacancy pairs $[\{Sr''_{Ce} - V_O^{\cdot\cdot}\}^{x}]$ [37,38]. Consequently activation energy increases and hence ionic conductivity decreases.

For compositions with $y \leq 0.04$, first two factors seem to dominate leading to an increase in ionic conductivity. For $y > 0.04$, the later two factors may start dominating causing a decrease in the ionic conductivity. $Y = 0.04$ seems to be an optimum value for molar concentration of Sr^{2+} which gives the maximum conductivity. Ionic conductivity increases also due to scavenging effect of strontium. The observed trend in the conductivity values may also be partly due to the same trend found in the average grain size of these samples mentioned earlier. Since conductivity of $Ce_{0.89}La_{0.07}Sr_{0.04}O_{1.925}$ composition is comparable to the highest conductivity reported for SDC and GDC, use of this material as a solid electrolyte for intermediate temperature solid oxide fuel cells will reduce the cost drastically. Its compatibility with other cell components, however, is necessary for its application in IT-SOFC and this need to be checked.

4. Conclusions

Samples of ceria co-doped with La and Sr, $Ce_{1-x-y}La_xSr_yO_{2-\{x/2+y\}}$ $\{(x = 0.15, y = 0), (x = 0.11, y = 0.02), (x = 0.07, y = 0.04)$ and $(x = 0.03, y = 0.06)\}$ having same number of oxygen vacancies $(x/2 + y)$ have been prepared by citrate-nitrate auto-combustion method. Density obtained by sintering at 1350 °C is more than 95% of theoretical density. It has been found that the average radius of oxygen vacancy formed by divalent and trivalent dopant cations in co-doped lanthanum and strontium systems is an important parameter for estimation of lattice parameter in this system. $Ce_{0.89}La_{0.07}Sr_{0.04}O_{1.925}$ shows higher conductivity (20 times) and lower activation energy than that of ceria doped with lanthanum only having the same number of oxygen vacancies This is also higher than the maximum value reported in the system, SDC and GDC. This increase in ionic conductivity is mainly due to decrease in grain boundary resistance.

Acknowledgement

Thanks are due to Department of Science and Technology, New Delhi for financial support.

References

[1] O. Yamamoto, Electrochim. Acta 45 (2000) 2423–2435.
[2] T.P. Chen, J.D. Wright, K. Krist, in: U. Stimming, S.C. Singhal, H. Tagawa, W. Lehnert (Eds.), SOFC V, The Electrochemical Society, Pennington, NJ, 1997, p. 69. PV 97-40.
[3] B.C.H. Steele, J. Mater. Sci. 36 (2001) 1053–1068.
[4] P. Holtappels, F.W. Poulsen, M. Mogensen, Solid State Ionics 135 (2000) 675–679.
[5] H.L. Tuller, in: H. Tuller, J. Schoonman, I. Riess (Eds.), Oxygen Ion and Mixed Conductors and Their Technological Applications, Kluwer (NATO ASI Series), Dordrecht, 2000, pp. 245–270.
[6] L. Minervini, M.O. Zacate, R.W. Grimes, Solid State Ionics 116 (1999) 339–349.
[7] T.H. Etsell, S.N. Flengas, Chem. Rev. 70 (1970) 339–376.
[8] H. Rickert, Electrochemistry of Solids. An Introduction, Springer-Verlag, Berlin, 1982.
[9] V.N. Chebotin, M.V. Perfilyev, Electrochemistry of Solid Electrolytes, Khimiya, Moscow, 1978.
[10] M.V. Perfilyev, A.K. Demin, B.L. Kuzin, A.S. Lipilin, High-temperature Electrolysis of Gases, Nauka, Moscow, 1988.
[11] V.V. Kharton, E.N. Naumovich, A.A. Vecher, J. Solid State Electrochem 3 (1999) 61–81.
[12] H. Inaba, H. Tagawa, Solid State Ionics 83 (1996) 1–16.
[13] H.J.M. Bouwmeester, A.J. Burggraaf, in: A. Burggraaf, L. Cot (Eds.), Fundamentals of Inorganic Membrane Science and Technology, Elsevier, Amsterdam, 1996, pp. 435–528.
[14] N.M. Sammes, G.A. Tompsett, H. Nafe, F. Aldinger, J. Eur. Ceram. Soc. 19 (1999) 1801–1826.
[15] M. Mogensen, N.M. Sammes, G.A. Tompsett, Solid State Ionics 129 (2000) 63–94.
[16] J.V. Herle, D. Seneviratne, A.J. McEvoy, J. Eur. Ceram. Soc. 19 (1999) 837–841.
[17] H. Yoshida, H. Deguchi, K. Miura, M. Horiuchi, Solid State Ionics 140 (2001) 191–199.
[18] H. Yoshida, T. Inagaki, K. Miura, M. Inaba, Z. Ogumi, Solid State Ionics 160 (2003) 109–116.
[19] S. Lubke, H.D. Wiemhofer, Solid State Ionics 117 (1999) 229–243.
[20] N. Kim, B.H. Kim, D. Lee, J. Power Sources 90 (2000) 139–143.
[21] F.Y. Wang, S. Chen, Q. Wang, S. Yu, S. Cheng, Catal. Today 97 (2004) 189–194.
[22] Tsung-Her Yeh, Chen-Chia Chou, Phys. Scr. T129 (2007) 303–307.
[23] S. Basu, P. Sujata Devi, H.S. Maiti, J. Mater. Res. 19 (2004) 3162–3171.
[24] N.K. Singh, P. Singh, M.K. Singh, D. Kumar, O. Parkash, Solid State Ionics 192 (2011) 431–434.
[25] S.J. Hong, A.V. Virkar, J. Am. Ceram. Soc. 78 (1995) 433–439.
[26] T.H. Yeh, W.C. Hsu, C.C. Chou, J. Phys. IV 128 (2005) 213–219.
[27] B.C.H. Steele, Solid State Ionics 180 (2009) 681–687.
[28] E. Ruiz-Trejo, A. Benitez-Rico, S. Gomez-Reynoso, M. Angeles-Rosas, J. Electrochem. Soc. 154 (4) (2007) A258–A262.
[29] N. Cioatera, V. Parvulescu, A. Rolle, R.N. Vannier, Solid State Ionics 180 (2009) 681–687.
[30] R. Gerhardt, A.S. Nowick, M.E. Mochel, I. Dumler, J. Am. Ceram. Soc. 69 (1986) 647–651.
[31] R. Gerhardt, A.S. Nowick, J. Am. Ceram. Soc. 69 (1986) 641–646.
[32] M.J. Verkerk, B.J. Middlehuis, A.J. Burggraaf, Solid State Ionics 6 (2) (1982) 159–170.
[33] G. Bryan Balazas, S. Robert Glass, Solid State Ionics 76 (1995) 155–162.
[34] Y.-P. Fu, S.-H. Chen, J.-J. Huang, Int. J. Hydrogen Energy 35 (2010) 745–752.
[35] H. Yamamura, E. Katoh, M. Ichikawa, K. Kakinuma, T. Mori, H. Haneda, Electrochemistry 68 (2000) 455–459.
[36] D.J. Kim, J. Am. Ceram. Soc. 72 (1989) 1415–1421.
[37] V. Butler, C.R.A. Catlow, B.E.F. Fender, J.H. Harding, Solid State Ionics 8 (1983) 109–113.
[38] J.A. Kilner, Solid State Ionics 8 (1983) 201–207.